Version of Record: https://www.sciencedirect.com/science/article/pii/S0022169417307369
Manuscript_c4b305a3f6796c9b8bc3f3452bfaa9cd

Analyzing the uncertainty of ensemble-based gridded observations in land surface simulations and drought assessment

Ali Ahmadalipour* and Hamid Moradkhani

Water Resources and Remote Sensing Lab, Department of Civil and Environmental Engineering, Portland State University, Portland, OR

*Corresponding author: aahmad2@pdx.edu

© 2017 published by Elsevier. This manuscript is made available under the Elsevier user license
https://www.elsevier.com/open-access/userlicense/1.0/

Abstract

Hydrologic modeling is one of the primary tools utilized for drought monitoring and drought early warning systems. Several sources of uncertainty in hydrologic modeling have been addressed in the literature. However, few studies have assessed the uncertainty of gridded observation datasets from a drought monitoring perspective. This study provides a hydrologic modeling oriented analysis of the gridded observation data uncertainties over the Pacific Northwest (PNW) and its implications on drought assessment. We utilized a recently developed 100-member ensemble-based observed forcing data to simulate hydrologic fluxes at 1/8° spatial resolution using Variable Infiltration Capacity (VIC) model, and compared the results with a deterministic observation. Meteorological and hydrological droughts are studied at multiple timescales over the basin, and seasonal long-term trends and variations of drought extent is investigated for each case. Results reveal large uncertainty of observed datasets at monthly timescale, with systematic differences for temperature records, mainly due to different lapse rates. The uncertainty eventuates in large disparities of drought characteristics. In general, an increasing trend is found for winter drought extent across the PNW. Furthermore, a ~3% decrease per decade is detected for snow water equivalent (SWE) over the PNW, with the region being more susceptible to SWE variations of the northern Rockies than the western Cascades. The agricultural areas of southern Idaho demonstrate decreasing trend of natural soil moisture as a result of precipitation decline, which implies higher appeal for anthropogenic water storage and irrigation systems.

Keywords: Pacific Northwest, Drought, Uncertainty, Land Surface Modeling, VIC

1. Introduction

Drought, defined as an extended period of moisture deficiency in the land surface, is among the costliest natural hazards with profound socioeconomic impacts (Dai, 2011; Livneh and Hoerling, 2016; Yan et al., 2016). Therefore, drought monitoring and drought early warning systems are crucial for water resources management and mitigating the impacts of droughts (Ahmadalipour et al., 2017c; Otkin et al., 2014; Pozzi et al., 2013).

Notwithstanding the severe economic, social, and ecological impacts of drought, it is among the least understood natural hazards due to the complexity and diversity in drought origins, obscure mechanisms for drought development and recovery, and multiscale (temporal and spatial) advancement and demise of drought (Hobbins et al., 2016; Kam et al., 2014; Vicente-Serrano et al., 2015; Wang et al., 2016). Furthermore, it is reported that the anthropogenic warming and climate change will alter the hydro-meteorological patterns and seasonal hydrologic cycles, consequently affecting drought characteristics (Ahmadalipour et al., 2016; Diffenbaugh et al., 2015; Duffy et al., 2015; Mishra and Coulibaly, 2009).

During the past decade, land surface modeling of hydrological cycle has received profound attention for drought monitoring purposes (Mishra and Singh, 2011; Svoboda et al., 2002; Xia et al., 2012). However, the existence of several sources of uncertainty makes the monitoring and prediction of drought a challenging process. Focusing on the epistemic uncertainties, several components contribute to the uncertainty in hydrologic modeling. Various studies have assessed some of these sources of uncertainty from a modeling perspective; such as model parameterization and calibration (Brigode et al., 2013), initial conditions (Abaza et al., 2014; Yan et al., 2017), model structure (Cai et al., 2014; Najafi et al., 2011; Najafi and Moradkhani, 2015; Samaniego et al., 2016), or a combination of the above (Bennett et al., 2012; Mendoza et al., 2015; Mizukami et al., 2016). Some other studies have pointed out the uncertainty raised due to forcing uncertainty for medium-range seasonal forecasts (Mo and Lyon, 2015; Shukla et al., 2016) to long-term decadal projections (Ahmadalipour et al., 2017a, 2016; Zhao and Dai, 2015). Moreover, the impacts of bias correction and downscaling methods on hydro-climatological portrayals have also been assessed (Ahmadalipour et al., 2017b; Ficklin et al., 2016; Gutmann et al., 2014).

In addition to the uncertainties of hydrologic modeling, drought monitoring can be challenging due to the differences among drought indices and timescales. Various drought indices consider different variables and therefore, there is a discrepancy between the onset and intensity of drought from different indices (Anderson et al., 2013; McEvoy et al., 2016). It is also worth noting that drought does not always have the same origin and reason, making the detection of drought onset and termination (recovery) more intricate. For instance, for the case of hydrological drought, a drought event may be classified as a rain-to-snow-season drought, cold/warm snow season drought, or snowmelt drought, as explained by Van Loon (2015).

Although Pacific Northwest (PNW) US is known for its abundant water, it has suffered severe droughts with significant socioeconomic impacts (Shukla et al., 2011). A few studies have assessed historical drought characteristics over the PNW to understand the causes of drought and its relationship with atmospheric teleconnections, and to improve drought predictability (Abatzoglou et al., 2014; Cooper et al., 2016; Yan et al., 2017). Some other studies have assessed future drought projections in the region (Ahmadalipour et al., 2017a). Recently, Xiao et al. (2016) utilized Variable Infiltration Capacity (VIC) model for the period of 1920-2013 to study drought over the PNW based on the total soil moisture variability.

The current study conducts a land surface modeling to analyze the patterns of drought over the Pacific Northwest using different observational datasets in order to diagnose the effects of observational choice on hydro-meteorological portrayals and drought. Our analysis benefits from the availability of a fine-resolution ensemble-based observational dataset of meteorological forcing. Meteorological and hydrological droughts are studied using drought indices at various timescales as well as the actual net moisture acquired from the land surface model outputs.

2. Study Area and Data

The study is conducted over the Pacific Northwest (PNW) US which covers the Columbia River Basin as well as the western coastal drainages. It is among the largest river basins in the US, covering portions of seven states in the western US (Washington, Oregon, Idaho, Montana, Wyoming, Nevada, and Utah) and parts of British Columbia in western Canada. Diverse climate and complex terrain is found across the basin, from low valley moist coastal regions at the western parts receiving annual precipitation of more than 2000 mm to semi-arid areas at the southeastern parts of the basin with less than 400 mm annual precipitation.

In general, the gridded observation datasets are generated by interpolating data from various gauge observations and accounting for elevation variations, lapse rate, etc. Thus, the gridded observation datasets can be affected by the following factors:

- The gauge stations that are included
- The interpolation technique
- The elevation chosen for each grid
- The temperature lapse rate

- The start and end time of the day (00UTC or local time)

Therefore, various gridded observations are different from each other as they do not necessarily employ similar methodology. In general, the deterministic gridded observations assign a single value to each grid, which would represent the majority of that grid. However, this may be impractical for the areas with diverse topography and regions subject to orographic effects. Therefore, the application of ensemble observation datasets would be useful for characterizing such uncertainty.

The gridded ensemble precipitation and temperature at 1/8° spatial resolution is utilized at a daily temporal resolution. The dataset has been developed by Newman et al. (2015) (hereafter represented by “N15”) which consists of 100 ensemble members of daily precipitation, mean temperature, and daily temperature range covering the historical period of 1980-2012. Various gauge observations and different probabilistic interpolation techniques were employed for developing the dataset.

Besides the ensemble observation, deterministic gridded observational dataset developed by Livneh et al. (2013) (hereafter represented by “L13”) is also utilized. L13 dataset has a spatial resolution of 1/16° (~6km in the north-south direction) and covers the historical period of 1915-2011. It consists of daily precipitation, maximum and minimum near surface air temperature, and wind speed, all of which are required to run the VIC model.

Since N15 dataset does not provide data for wind speed, the wind data from L13 dataset is utilized for running VIC model for all cases. Furthermore, in order to objectively assess the uncertainty of observational data on hydrological fluxes, the L13 dataset is aggregated to 1/8° to match the spatial resolution of N15 data. In this study, we have used all the available daily data from N15 dataset (100 ensemble members and the ensemble mean for the period of 1980-2012) as well as daily L13 dataset for the period of 1950-2011. A summary of the gridded observation datasets is provided in Table 1.

Table 1. Summary of the characteristics of the gridded observation datasets utilized in this study; modified from Newman et al. (2015) and Henn et al. (2017).

----

3. Methodology

3.1. Hydrologic model

The Variable Infiltration Capacity (VIC) model is a physically-based semi-distributed macroscale hydrologic model (Liang et al., 1994). The land surface is modeled as uniform grids and the model parameterizes sub-grid variability of vegetation, land cover, and soil. VIC model has been successfully applied in numerous studies across the globe (Prudhomme et al., 2014; Shukla et al., 2013; Yuan et al., 2015) and over the PNW for hydrologic simulations and drought analysis (Najafi and Moradkhani, 2015; Xiao et al., 2016).

Here, we have used VIC model, version 4.2.c, with three soil layers at a daily time step and 1/8° spatial resolution to reconstruct historical hydrological fluxes over the PNW. A total of 6392 grids cover the study area at 1/8° spatial resolution. The model parameter files including soil properties, vegetation cover, and elevation are acquired from the VIC retrospective land surface dataset developed by Maurer et al. (2002). They performed a comprehensive calibration/validation of the model over the Conterminous United States, showed that the calibrated model performed accurately for streamflow and soil moisture simulations. In this study, VIC model was run in water balance mode for each of the 100 ensemble members as well as the ensemble mean of N15 dataset for the period of 1980-2012. The model was also implemented for the L13 forcing for the period of 1950-2011. Surface runoff, snow water equivalent (SWE), evapotranspiration, and three layers of soil moisture were extracted from the model outputs.

3.2. Drought analysis

The Standardized Precipitation Index (SPI) (Mckee et al., 1993) and the Standardized Runoff Index (SRI) (Shukla and Wood, 2008) were utilized to study meteorological and hydrological droughts, respectively. Both drought indices were calculated at two timescales of 3- and 6-month accumulation periods to better reflect intra-annual attributes of hydrologic cycle. The conventional distribution fitting procedures i.e., Gamma and Lognormal distributions which were used to fit to the precipitation data, are known to have few issues. For instance, the calculated drought index was subject to the choice of distribution. Moreover, the most suitable distribution could vary for different locations. The drought index calculated using parametric distributions is unbounded and it can result in very high and low values, which can impact long-term trends. Therefore, a non-parametric procedure is implemented in this study to calculate drought indices. In order to calculate the indices, precipitation and runoff of each grid were accumulated to the desired accumulation period, and the empirical Weibull plotting position (Weibull, 1939) was utilized (as a non-parametric approach which eliminates the parametric distribution selection and fitting procedure) as follows:

$$p(x_i) = \frac{i}{n+1}$$

where n is the sample size, i represents the rank of accumulated precipitation or runoff from the smallest, and $p(x_i)$ is the empirical probability. $p(x_i)$ is then transformed to a standardized normal distribution (with mean zero and unit standard deviation) to obtain the drought index. For each index and each timescale, drought extent in each month was calculated as the percentage of area having a drought index below -0.8, indicating moderate to extreme drought condition.

4. Results and Discussion

4.1. Hydro-meteorological fluxes

The first part of our analysis focuses on comparing the hydro-meteorological fluxes of deterministic L13 observation with the outputs of the ensemble of N15 dataset. This is performed at various temporal resolutions (i.e. monthly, seasonal and annual) to better address the differences and uncertainties. Figure 1 shows the spatial mean annual precipitation (Prec), mean air temperature (TMean), runoff, and evapotranspiration (Evap) over the PNW for the period of 1980-2012. The precipitation (Prec.) and mean temperature (TMean) are directly extracted from the gridded observation datasets. They are used as input to the VIC model in order to generate runoff and evapotranspiration, and these two variables are plotted in the bottom two plots. The light blue plots present 100 members of the N15 data and the bold dark blue line indicates the results for the ensemble mean of N15 dataset. As it can be seen, N15 indicates higher precipitation and temperature than those from L13. The difference in temperature is more pronounced as all the ensemble members of N15 show about 0.5°C warmer air temperature than that of L13 observations. Having higher temperature and precipitation, N15 indicates about 50mm higher annual average evapotranspiration than L13 simulations. Nevertheless, datasets are more in agreement for annual mean runoff. In other words, L13 and the ensemble mean of N15 (shown in bold blue line) show similar annual runoff. The highest and lowest annual precipitation over the PNW are found in 1996 (~1200mm) and 1985 (~700mm), respectively.

Also, the lowest annual temperature is recorded in1985, and 1996 indicates the highest average runoff due to abundant precipitation.

Figure 1. Spatial mean annual precipitation, mean air temperature, runoff, and evapotranspiration over the Pacific Northwest for the period of 1980-2012.

The seasonal long-term mean of the hydro-meteorological variables are calculated for the period of 1980-2011, and the results are shown in Figure 2. The figure shows the long-term seasonal mean of climate variables in winter (JFM) and summer (JAS) for L13 and the ensemble mean of N15 dataset. From Figure 2, the highest precipitation in JFM and JAS are found at the western and northern parts of PNW, respectively. Similar seasonal spatial pattern is found for runoff. The warmest regions in winter (JFM) seems to be the western coastal areas, whereas eastern Washington and low valleys of southern Idaho indicate the highest temperatures in summer (JAS). The spatial pattern of evapotranspiration shows dependence on both temperature and runoff. For instance, the low valleys of southern Idaho indicates the lowest evapotranspiration in JAS due to limited water availability. Evapotranspiration of JFM seems to have similar spatial distribution as runoff with the highest values at western coastal areas. Therefore, southern Idaho and central parts of PNW (eastern parts of Oregon and Washington) are water-limited, whereas western coastal regions are energy-limited (Milly and Dunne, 2002; Najafi et al., 2011).

Figure 2. Long-term seasonal mean of hydro-meteorological variables for the period of 1980-2011.

Although both datasets seem to have similar spatial patterns for long-term mean condition, the differences are not clear from Figure 2. Therefore, results of both datasets are plotted against each other using scatterplots and shown in Figure S1. The figure shows that the long-term seasonal mean temperature of N15 exceeds L13 dataset by about 2°C in some grids. Furthermore, JFM evapotranspiration of N15 is higher than L13 in almost all grids. For long-term average runoff, N15 indicates higher runoff than L13 in JFM, and vice versa for JAS.

Figures 1 and 2 represented annual and seasonal spatial and temporal mean of hydro-meteorological variables, respectively. Besides the mean condition, it is also important to understand the differences for extreme conditions. Therefore, the 90^{th} percentile of each variable during the period of 1980-2011 is extracted for each month for L13 as well as each ensemble member of N15 dataset, and the results are shown in Figure 3. The uncertainty of observation datasets is more noticeable in monthly extremes, and diverse patterns are found among different months. For instance, comparing N15 and L13 datasets, the former shows higher extreme precipitation and temperature in JFM, while it indicates lower values than L13 in spring and summer (MMJJAS). This seasonal pattern is similarly replicated in runoff with higher uncertainty for the N15 ensemble. The 90^{th} percentile values of evapotranspiration (/SWE) for N15 is always higher (/lower) than the L13 results. For soil moisture (SM), N15 shows higher SM values than L13 in the first four months of the year (JFMA) and stays lower than L13 for rest of the months.

Figure 3. Monthly 90th percentile values of each hydroclimatic variable from N15 (blue) and L13 data (red) for the period of 1980-2011.

Due to the significant role of SWE in hydrological processes (especially for spring runoff and soil moisture), simulations of SWE from the VIC model are analyzed separately and the results are shown in Figure 4. The top rows of Figure 4 represent the long-term seasonal mean SWE from N15 and L13 datasets for the period of 1982-2011, and the bottom plot indicates annual mean SWE over PNW. Two main SWE resources in PNW are the Rocky Mountains and Cascades located in east and west sides of the PNW, respectively. Considering the bottom plot, L13 indicates higher SWE than N15. Furthermore, focusing on long-term trend of annual SWE from L13 simulations, a significant linear trend of -40mm/decade (about -3% of annual mean SWE) is found for spatial mean SWE over the PNW for the period of 1950-2011.

Figure 4. (top) Long-term seasonal mean SWE for the period of 1982-2011; (bottom) spatial mean annual SWE over the basin for each dataset.

Decreasing SWE may have substantial impacts on spring runoff and soil moisture, which may lead to intensified drought conditions (Safeeq et al., 2014). Previous studies have investigated the decreasing trend of SWE and snow cover in western US (Kapnick and Hall, 2012; Mote et al., 2016) and Sierra Nevada (Margulis et al., 2016; Rittger et al., 2016). It has been shown that anthropogenic warming and earlier spring onset have considerable role on the decreasing trend of SWE (Pierce and Cayan, 2013).

In order to better understand the regional trends of SWE, its monthly variations and long-term trends are analyzed for the western Cascades, northern Rockies, and the entire PNW for the period of 1950-2011 using L13 simulations. Results of the long-term trends of SWE are shown in Figure 5. In the figure, the left plots show monthly spatial mean SWE from L13 simulations. The long-term linear trends are calculated for winter and spring (DJFMAM) and the percentage change of SWE per decade is shown in the right bar plots. In most cases, monthly SWE indicates about -2% decrease per decade. Considering western Cascades, SWE indicates decreasing pattern for all months. Whereas, the Northern Rockies and PNW indicate slightly increasing SWE in December and January. From the left plots, it can be seen that the early 1970s experienced abundant SWE (especially in Cascades), followed by about two decades of lower SWE records. Considering monthly variations and long-term trends, PNW seems to be more sensitive to SWE variations in Northern Rockies than western Cascades. This is confirmed when considering the below-normal state of SWE between 2009-2011 for both PNW and Northern Rockies, while the Cascades shows normal SWE conditions in the same period.

\-----------------------

Figure 5. (left) Monthly SWE (mm) from L13 dataset for the period of 1950-2011; (right) long-term linear trend of monthly SWE presented as the percentage change per decade.

\-----------------------

The last hydrologic comparison between L13 and N15 observations is conducted on monthly simulations of each variable, and the results are shown in Figure 6 using density-type scatterplots. Figure 6 presents a comparison of monthly simulations of L13 and the ensemble mean of N15 for each grid during the 30-year historical period of 1982-2011. Each plot is generated using more than 2.3×10^6 data records (6392grids × 30years × 12months). The results of previous analysis are confirmed here with higher temperature and evapotranspiration and lower SWE of N15 than L13. Figure 6 illustrates the discrepancy between the observation datasets at monthly timescale (suitable for drought assessment), which would be worse at finer temporal resolutions such as daily timescale (suitable for heatwave or flood analysis). For instance, N15 shows more than 5°C higher temperature than L13 in low temperatures, whereas datasets seem to be more in agreement at high temperatures. Although spatial mean annual runoff of N15 and L13 (presented in Figure 1) were similar to each other, monthly runoff shows vast differences at grid-scale comparison.

Figure 6. Density-type scatterplots of monthly simulations of L13 and N15 observations for 30-year period of 1982-2011. In the plots, each axis is divided into 100 bins and the number of occurrences in each 2D bin is indicated by the colorbar.

4.2. Drought simulation

The SPI and SRI are calculated at 3- and 6-month accumulation periods starting at each month and for each grid in the PNW. This is carried out for L13 data for the period of 1950-2011 and for each of the 100 ensemble members as well as the ensemble mean of N15 dataset for the period of 1980-2012. Drought extent is calculated for each month and the average drought extent of PNW in each season (JFM, AMJ, JAS, and OND) is plotted in Figures 7 and S2 for 6- and 3-month accumulation periods, respectively. Drought extent of both timescales seem to follow similar patterns for each season. However, the figures show large differences between the L13 and N15 simulations. Among the four seasons, the N15 and L13 simulations seem to be more similar in spring and summer, especially for SPI-3 in AMJ.

Figure 7. Time series of mean seasonal drought extent of PNW at 6-month accumulation period for L13 and N15 simulations.

The decreasing SWE during 1970s and 1980s has clearly affected the drought extent of that period. This can be seen in the substantial increase of summer (JAS) drought extent (shown in Figures 7 and S2). Recently, Ahmadalipour et al. (2017a) investigated the impacts of climate change on the meteorological and hydrological droughts of the Willamette Basin, located at the western parts of the Pacific Northwest. They concluded that the earlier snowmelt onset and lower snowpack accumulation (both affected by climate change) will significantly affect streamflow and drought characteristics, especially in distant future.

To better understand the role of observational uncertainty on drought, the long-term cumulative distribution function (CDF) of each drought extent time-series is generated for the period of 1981-2011 for L13 and N15 simulations, and the results are plotted in Figure 8 for each case. From the figure, L13 shows higher drought extent than N15 in JFM and OND for all cases. For instance, the median of L13 drought extent in OND is about 10% higher than that for N15 simulations. The differences are lower in spring and summer. Focusing on the median of drought extent CDFs and comparing different seasons, the lowest drought extent in PNW happens in spring (AMJ) with about 16% of PNW experiencing drought.

Figure 8. Long-term CDF of drought extent in PNW for each season and each drought index during the period of 1981-2011.

In order to assess the long-term changes of drought extent over PNW, the linear trend of drought extent is calculated for each index in each season, and the results are plotted in Figure 9. The trend of L13 drought extent is calculated once for 1951-2011 to reveal 60-year long-term trends and once for 1981-2011 to be compared with N15 results. For the period of 1981-2011, both L13 and N15 indicate increasing drought extent in AMJ and JFM for most cases. However, L13 shows decreasing drought extent in AMJ for the longer period (1951-2011). In general, L13 indicates the largest (both negative and positive) trend values for drought extent. SRI-3 shows increasing drought extent in most seasons among all cases. The decadal trend of 2% increase in drought extent is significant in the region. For instance, the JFM drought extent in 1980s was about 15%, and the same in 2000s is above 25%. Considering the ~900,000 km^2 area of the region, the affected area by drought has increased more than 90,000 km^2 in the past decades.

Figure 9. Linear trend of drought extent in each season presented as the percentage change per decade.

Among the regions in PNW, the low valleys of southern Idaho (eastern parts of southern Snake River Basin) is covered with agricultural areas and farmlands. The region receives low precipitation and high temperature. Hydrological characteristics of this region is exclusively investigated in order to diagnose the impacts of hydrological changes on agriculture. Therefore, apart from drought indices and drought extent, the variation of actual net moisture is studied for low valleys of southern Idaho as a means to provide a physical representation for moisture availability. We define net moisture as the sum of incoming moisture (precipitation, soil moisture, and SWE) minus evapotranspiration, as follows:

$$Net\ Moisture = Prec + SM + SWE - Evap$$

Since the region receives low SWE, the main incoming moisture would be precipitation and soil moisture. Here, the variability of net moisture is studied during the growing season (MJJAS) and the results are provided in Figure 10. The figure shows spatial mean net moisture and its main input components (i.e. Prec. and SM) for the period of 1982-2011 for both L13 and the ensemble mean of N15 simulations. From the top panel of Figure 10, L13 indicates higher net moisture than N15, mainly because the latter possesses higher evapotranspiration. Both datasets exhibit decreasing trends of about 7% per decade for the net moisture. Considering the bottom plot, decreasing trend is found for both precipitation and top layer soil-moisture (which is crucial for vegetation health and agricultural yield). A decreasing trend in soil moisture implies higher demand for anthropogenic water storage and irrigation systems. The decreasing moisture trend would also impose damages to vegetation. Recently, Ahmadalipour et al. (2017c) utilized Vegetation Health Index (VHI) (Kogan, 1995) calculated from remotely sensed observations of Advanced Very High Resolution Radiometer (AVHRR) satellite at a weekly timescale during the growing season over the contiguous United States (CONUS) for the period of 1982-2015. Their results also confirm the aggravating drought and exacerbating vegetation health condition for the region.

Figure 10. Variability of net moisture (top) and its input components (bottom) over the agricultural areas of southern Idaho during the growing season (MJJAS) for the period of 1982-2011.

From Figure 10, the temporal variations of precipitation and top layer soil moisture during the growing season follow very similar patterns, and a correlation coefficient of 0.96 is found between them. Considering the underlying land-atmosphere feedbacks and the attributable impacts of soil moisture on aridity and temperature extremes (Berg et al., 2016; Whan et al., 2015), the decreasing soil moisture pattern not only poses drought and harmful effect on vegetation health, it also alters the hydrological processes and water cycle dynamics (Mishra et al., 2017; Schwingshackl et al., 2017). Understanding the feedbacks and inter-relationships of hydro-meteorological variables and fluxes has received more attention in recent years, especially given the availability of more accurate global satellite observations (McColl et al., 2017; Whan et al., 2015).

This study revealed the importance of considering observation uncertainty for assessing hydrological fluxes and drought monitoring purposes. Although some of the previous studies have investigated the meteorological differences among observed datasets (Henn et al., 2017; Lundquist et al., 2015; Newman et al., 2015), few studies addressed the consequences of such disparities on drought modeling (Trenberth et al., 2014).

Assessing the long-term variations and trends of the hydrological variables indicates a distinct changing pattern. It has been shown that the increase in temperature has crucial implications on different variables such as snow water equivalent, evapotranspiration, and soil moisture, among others (Gergel et al., 2017; Sima et al., 2013). The changes of hydro-meteorological variables are reflected in drought characteristics, while altering intensity, severity and impacts of droughts. For instance, the idea of “snow drought” which refers to the reduced snow accumulation hence drought, has recently received extensive attention, especially after the unprecedented 2011-2016 California drought (Cooper et al., 2016; Harpold et al., 2017).

Besides the areal extent of drought, which was elaborated in this study, other drought characteristics (e.g. intensity, duration, and frequency) have been assessed in many other studies across the globe, and it has been discussed that droughts have been exacerbated in many regions (Chen and Sun, 2017; Dai and Zhao, 2016; Zhai et al., 2017). The results of this study revealed distinct long-term patterns among different seasons for SWE and drought extent. Diverse seasonal patterns were detected for different seasons, highlighting the necessity of seasonal analysis for similar assessments.

The observational datasets are utilized as the basis for various applications such as evaluating, bias correction, and statistical downscaling of climate models, or improving the accuracy and reliability of hydrologic forecasts through post-processing methods (Ahmadalipour et al., 2015; Khajehei and Moradkhani, 2017; Robertson et al., 2013). Thus, the observation uncertainty may affect such processes, and it should be investigated with more attention for these applications, especially for micro- to meso-scale extreme events of shorter timescales. One of the main points of this study was to show how minor differences in daily precipitation and temperature of gridded observation datasets can yield to disparities for other hydrologic variables (e.g. SWE or ET) and drought.

The results also showed that the forcing data uncertainty is different across timescales and it increases as the timescale becomes shorter. In other words, the observation uncertainty is expected to be lower at annual timescale compared to seasonal and monthly timescales. Therefore, the implications of observation uncertainty would be different for different phenomena including aridity, drought, medium-range hydrologic forecast, and flood, possessing long to short timescales, respectively. Results of this study showed that observation uncertainty is large in most regions of PNW, especially in wet coastal regions. Therefore, it is necessary to consider such uncertainties for analyzing long-term changes or short-term hydrological monitoring and forecast.

Droughts impose about $6-8 billion damage in the United States each year (Smith and Matthews, 2015). The impacts are not only economical, rather the environmental and ecological impacts are more severe (Crausbay et al., 2017). Droughts can also increase the risk of wildfires, which is a serious issue for the densely vegetated areas of the Pacific Northwest US (Gudmundsson et al., 2014). Therefore, drought monitoring and prediction systems are vital for mitigating such impacts and for subsiding its social and ecological consequences. Understanding and characterizing different sources of uncertainty in drought monitoring systems will help improve the accuracy of drought onset and recovery detection (Yan et al., 2017).

5. Summary and Conclusion

This study provided an assessment of hydro-meteorological fluxes and historical droughts over the PNW. We employed VIC model at 1/8° spatial resolution for a 100-member ensemble of observed forcing data (N15) during the period of 1980-2012 as well as a deterministic observation (L13) for the period of 1950-2011, and compared the model outputs at various timescales for different variables. Meteorological and hydrological droughts were investigated using SPI and SRI, respectively, and drought extent was assessed for each case. The main findings of our study are summarized as follows:

- Observation forcing uncertainty is high at monthly timescale, which eventuates in high disparities in hydrologic fluxes and drought characteristics.
- The N15 simulations indicate higher temperature and evapotranspiration and lower SWE than the L13 data. The difference can be as high as 6°C in monthly low temperatures and 150mm for monthly precipitation.
- A -3% decrease per decade is found for annual SWE over the PNW. Two major SWE suppliers of the region are the western Cascades and the northern Rockies, and PNW shows to be more sensitive to SWE variations of the latter.
- The L13 indicates higher drought extent than N15 simulations in JFM and OND. The long-term drought extent indicates an increasing trend in JFM for most cases.
- Focusing on the agricultural areas of southern Idaho, precipitation and top-layer soil moisture indicate a decreasing trend for the past 30 years, causing about 7% decrease per decade for the net moisture of the region.

Acknowledgement

The authors are thankful for the financial support provided by NOAA-MAPP program, grant NA140AR4310234.

References

Abatzoglou, J.T., Rupp, D.E., Mote, P.W., 2014. Seasonal Climate Variability and Change in the Pacific Northwest of the United States. J. Clim. 27, 2125–2142. doi:10.1175/JCLI-D-13-00218.1

Abaza, M., Anctil, F., Fortin, V., Turcotte, R., 2014. Sequential streamflow assimilation for short-term hydrological ensemble forecasting. J. Hydrol. 519, 2692–2706.

Ahmadalipour, A., Moradkhani, H., Demirel, M.C., 2017a. A comparative assessment of projected meteorological and hydrological droughts: Elucidating the role of temperature. J. Hydrol. 553, 785–797. doi:10.1016/j.jhydrol.2017.08.047

Ahmadalipour, A., Moradkhani, H., Rana, A., 2017b. Accounting for downscaling and model uncertainty in fine-resolution seasonal climate projections over the Columbia River Basin. Clim. Dyn. 1–17. doi:10.1007/s00382-017-3639-4

Ahmadalipour, A., Moradkhani, H., Svoboda, M., 2016. Centennial drought outlook over the CONUS using NASA-NEX downscaled climate ensemble. Int. J. Climatol. 37, 2477–2491. doi:10.1002/joc.4859

Ahmadalipour, A., Moradkhani, H., Yan, H., Zarekarizi, M., 2017c. Remote Sensing of Drought: Vegetation, Soil Moisture and Data Assimilation, in: Remote Sensing of Hydrological Extremes. Springer International Publishing Switzerland, pp. 121–149.

Ahmadalipour, A., Rana, A., Moradkhani, H., Sharma, A., 2015. Multi-criteria evaluation of CMIP5 GCMs for climate change impact analysis. Theor. Appl. Climatol. doi:10.1007/s00704-015-1695-4

Anderson, M.C., Hain, C., Otkin, J., Zhan, X., Mo, K., Svoboda, M., Wardlow, B., Pimstein, A., 2013. An Intercomparison of Drought Indicators Based on Thermal Remote Sensing and NLDAS-2 Simulations with U.S. Drought Monitor Classifications. J. Hydrometeorol. 14, 1035–1056. doi:10.1175/JHM-D-12-0140.1

Bennett, K.E., Werner, A.T., Schnorbus, M., 2012. Uncertainties in Hydrologic and Climate Change Impact Analyses in Headwater Basins of British Columbia. J. Clim. 25, 5711–5730. doi:10.1175/JCLI-D-11-00417.1

Berg, A., Findell, K., Lintner, B., Giannini, A., Seneviratne, S.I., Van Den Hurk, B., Lorenz, R., Pitman, A., Hagemann, S., Meier, A., 2016. Land-atmosphere feedbacks amplify aridity increase over land under global warming. Nat. Clim. Chang.

Brigode, P., Oudin, L., Perrin, C., 2013. Hydrological model parameter instability: A source of additional uncertainty in estimating the hydrological impacts of climate change? J. Hydrol. 476, 410–425.

Cai, X., Yang, Z.-L., Xia, Y., Huang, M., Wei, H., Leung, L.R., Ek, M.B., 2014. Assessment of simulated water balance from Noah, Noah-MP, CLM, and VIC over CONUS using the NLDAS test bed. J. Geophys. Res. Atmos. 119, 13,751-13,770. doi:10.1002/2014JD022113.Received

Chen, H., Sun, J., 2017. Anthropogenic warming has caused hot droughts more frequently in

China. J. Hydrol. 544, 306–318.

Cooper, M.G., Nolin, A.W., Safeeq, M., 2016. Testing the recent snow drought as an analog for climate warming sensitivity of Cascades snowpacks. Environ. Res. Lett. 11, 84009.

Crausbay, S.D., Ramirez, A.R., Carter, S.L., Cross, M.S., Hall, K.R., Bathke, D.J., Betancourt, J.L., Colt, S., Cravens, A.E., Dalton, M.S., 2017. Defining ecological drought for the 21st century. Bull. Am. Meteorol. Soc.

Dai, A., 2011. Drought under global warming: a review. Wiley Interdiscip. Rev. Clim. Chang. 2, 45–65.

Dai, A., Zhao, T., 2016. Uncertainties in historical changes and future projections of drought. Part I: estimates of historical drought changes. Clim. Change 1–15.

Diffenbaugh, N.S., Swain, D.L., Touma, D., 2015. Anthropogenic warming has increased drought risk in California. Proc. Natl. Acad. Sci. 112, 201422385. doi:10.1073/pnas.1422385112

Duffy, P.B., Brando, P., Asner, G.P., Field, C.B., 2015. Projections of future meteorological drought and wet periods in the Amazon. Proc. Natl. Acad. Sci. 112, 201421010. doi:10.1073/pnas.1421010112

Ficklin, D.L., Abatzoglou, J.T., Robeson, S.M., Dufficy, A., 2016. The influence of climate model biases on projections of aridity and drought. J. Clim.

Gergel, D.R., Nijssen, B., Abatzoglou, J.T., Lettenmaier, D.P., Stumbaugh, M.R., 2017. Effects of climate change on snowpack and fire potential in the western USA. Clim. Change 141, 287–299.

Gudmundsson, L., Rego, F.C., Rocha, M., Seneviratne, S.I., 2014. Predicting above normal wildfire activity in southern Europe as a function of meteorological drought. Environ. Res. Lett. 9, 84008.

Gutmann, E., Pruitt, T., Clark, M.P., Brekke, L., Arnold, J.R., Raff, D.A., Rasmussen, R.M., 2014. An intercomparison of statistical downscaling methods used for water resource assessments in the United States. Water Resour. Res. 50, 7167–7186.

Harpold, A.A., Dettinger, M., Rajagopal, S., 2017. Defining snow drought and why it matters, Eos, 98.

Henn, B., Newman, A.J., Livneh, B., Daly, C., Lundquist, J.D., 2017. An assessment of differences in gridded precipitation datasets in complex terrain. J. Hydrol. doi:http://dx.doi.org/10.1016/j.jhydrol.2017.03.008

Hobbins, M., Wood, A., McEvoy, D., Huntington, J., Morton, C., Verdin, J., Anderson, M., Hain, C., 2016. The Evaporative Demand Drought Index: Part I-Linking Drought Evolution to Variations in Evaporative Demand. J. Hydrometeorol.

Kam, J., Sheffield, J., Wood, E.F., 2014. Changes in drought risk over the contiguous United States (1901–2012): The influence of the Pacific and Atlantic Oceans. Geophys. Res. Lett. 41, 5897–5903.

Kapnick, S., Hall, A., 2012. Causes of recent changes in western North American snowpack. Clim. Dyn. 38, 1885–1899.

Khajehei, S., Moradkhani, H., 2017. Towards an improved ensemble precipitation forecast: A probabilistic post-processing approach. J. Hydrol. 546, 476–489.

Kogan, F.N., 1995. Application of vegetation index and brightness temperature for drought detection. Adv. Sp. Res. 15, 91–100.

Liang, X., Lettenmaier, D.P., Wood, E.F., Burges, S.J., 1994. A simple hydrologically based model of land surface water and energy fluxes for general circulation models. J. Geophys. Res. Atmos. 99, 14415–14428.

Livneh, B., Hoerling, M.P., 2016. The physics of drought in the US central great plains. J. Clim. 29, 6783–6804.

Livneh, B., Rosenberg, E.A., Lin, C., Nijssen, B., Mishra, V., Andreadis, K.M., Maurer, E.P., Lettenmaier, D.P., 2013. A Long-Term Hydrologically Based Dataset of Land Surface Fluxes and States for the Conterminous United States: Update and Extensions*. J. Clim. 26, 9384–9392. doi:10.1175/JCLI-D-12-00508.1

Lundquist, J.D., Hughes, M., Henn, B., Gutmann, E.D., Livneh, B., Dozier, J., Neiman, P., 2015. High-elevation precipitation patterns: Using snow measurements to assess daily gridded datasets across the Sierra Nevada, California. J. Hydrometeorol. 16, 1773–1792.

Margulis, S.A., Cortés, G., Girotto, M., Huning, L.S., Li, D., Durand, M., 2016. Characterizing the extreme 2015 snowpack deficit in the Sierra Nevada (USA) and the implications for drought recovery. Geophys. Res. Lett. 43, 6341–6349.

Maurer, E.P., Wood, A.W., Adam, J.C., Lettenmaier, D.P., Nijssen, B., 2002. A long-term hydrologically based dataset of land surface fluxes and states for the conterminous United States. J. Clim. 15, 3237–3251.

McColl, K.A., Alemohammad, S.H., Akbar, R., Konings, A.G., Yueh, S., Entekhabi, D., 2017. The global distribution and dynamics of surface soil moisture. Nat. Geosci. 10, 100–104.

McEvoy, D.J., Huntington, J.L., Hobbins, M.T., Wood, A., Morton, C., Verdin, J., Anderson, M., Hain, C., 2016. The Evaporative Demand Drought Index: Part II–CONUS-wide Assessment Against Common Drought Indicators. J. Hydrometeorol.

Mckee, T.B., Doesken, N.J., Kleist, J., 1993. The relationship of drought frequency and duration to time scales. AMS 8th Conf. Appl. Climatol. 179–184. doi:citeulike-article-id:10490403

Mendoza, P.A., Clark, M.P., Mizukami, N., Newman, A.J., Barlage, M., Gutmann, E.D., Rasmussen, R.M., Rajagopalan, B., Brekke, L.D., Arnold, J.R., 2015. Effects of hydrologic model choice and calibration on the portrayal of climate change impacts. J. Hydrometeorol. 16, 762–780.

Milly, P.C.D., Dunne, K.A., 2002. Macroscale water fluxes 2. Water and energy supply control of their interannual variability. Water Resour. Res. 38.

Mishra, A., Vu, T., ValiyaVeettil, A., Entekhabi, D., 2017. Drought Monitoring with Soil

Moisture Active Passive (SMAP) Measurements. J. Hydrol.

Mishra, A.K., Coulibaly, P., 2009. Developments in hydrometric network design: A review. Rev. Geophys. 47.

Mishra, A.K., Singh, V.P., 2011. Drought modeling – A review. J. Hydrol. 403, 157–175. doi:10.1016/j.jhydrol.2011.03.049

Mizukami, N., Clark, M.P., Gutmann, E.D., Mendoza, P.A., Newman, A.J., Nijssen, B., Livneh, B., Hay, L.E., Arnold, J.R., Brekke, L.D., 2016. Implications of the methodological choices for hydrologic portrayals of climate change over the contiguous United States: statistically downscaled forcing data and hydrologic models. J. Hydrometeorol. 17, 73–98.

Mo, K.C., Lyon, B., 2015. Global Meteorological Drought Prediction Using the North American Multi-Model Ensemble. J. Hydrometeorol. 16, 1409–1424. doi:10.1175/JHM-D-14-0192.1

Mote, P.W., Rupp, D.E., Li, S., Sharp, D.J., Otto, F., Uhe, P.F., Xiao, M., Lettenmaier, D.P., Cullen, H., Allen, M.R., 2016. Perspectives on the causes of exceptionally low 2015 snowpack in the western United States. Geophys. Res. Lett. 43.

Najafi, M.R., Moradkhani, H., 2015. Multi-model ensemble analysis of runoff extremes for climate change impact assessments. J. Hydrol. 525, 352–361. doi:10.1016/j.jhydrol.2015.03.045

Najafi, M.R., Moradkhani, H., Jung, I.W., 2011. Assessing the uncertainties of hydrologic model selection in climate change impact studies. Hydrol. Process. 25, 2814–2826. doi:10.1002/hyp.8043

Newman, A.J., Clark, M.P., Craig, J., Nijssen, B., Wood, A., Gutmann, E., Mizukami, N., Brekke, L., Arnold, J.R., 2015. Gridded ensemble precipitation and temperature estimates for the contiguous United States. J. Hydrometeorol. 16, 2481–2500.

Otkin, J. a., Shafer, M., Svoboda, M., Wardlow, B., Anderson, M.C., Hain, C., Basara, J., 2014. Facilitating the Use of Drought Early Warning Information through Interactions with Agricultural Stakeholders. Bull. Am. Meteorol. Soc. 141230123603006. doi:10.1175/BAMS-D-14-00219.1

Pierce, D.W., Cayan, D.R., 2013. The uneven response of different snow measures to human-induced climate warming. J. Clim. 26, 4148–4167.

Pozzi, W., Sheffield, J., Stefanski, R., Cripe, D., Pulwarty, R., Vogt, J. V, Heim Jr, R.R., Brewer, M.J., Svoboda, M., Westerhoff, R., 2013. Toward global drought early warning capability: Expanding international cooperation for the development of a framework for monitoring and forecasting. Bull. Am. Meteorol. Soc. 94, 776–785.

Prudhomme, C., Giuntoli, I., Robinson, E.L., Clark, D.B., Arnell, N.W., Dankers, R., Fekete, B.M., Franssen, W., Gerten, D., Gosling, S.N., 2014. Hydrological droughts in the 21st century, hotspots and uncertainties from a global multimodel ensemble experiment. Proc. Natl. Acad. Sci. 111, 3262–3267.

Rittger, K., Bair, E.H., Kahl, A., Dozier, J., 2016. Spatial estimates of snow water equivalent from reconstruction. Adv. Water Resour. 94, 345–363.

Robertson, D.E., Shrestha, D.L., Wang, Q.J., 2013. Post-processing rainfall forecasts from numerical weather prediction models for short-term streamflow forecasting. Hydrol. Earth Syst. Sci. 17, 3587.

Safeeq, M., Grant, G.E., Lewis, S.L., Kramer, M.G., Staab, B., 2014. A hydrogeologic framework for characterizing summer streamflow sensitivity to climate warming in the Pacific Northwest, USA. Hydrol. Earth Syst. Sci. 18, 3693–3710. doi:10.5194/hess-18-3693-2014

Samaniego, L., Kumar, R., Breuer, L., Chamorro, A., Flörke, M., Pechlivanidis, I.G., Schäfer, D., Shah, H., Vetter, T., Wortmann, M., 2016. Propagation of forcing and model uncertainties on to hydrological drought characteristics in a multi-model century-long experiment in large river basins. Clim. Change 1–15.

Schwingshackl, C., Hirschi, M., Seneviratne, S.I., 2017. Quantifying spatio-temporal variations of soil moisture control on surface energy balance and near-surface air temperature. J. Clim. doi:10.1175/JCLI-D-16-0727.1

Shukla, S., Roberts, J., Hoell, A., Funk, C.C., Robertson, F., Kirtman, B., 2016. Assessing North American multimodel ensemble (NMME) seasonal forecast skill to assist in the early warning of anomalous hydrometeorological events over East Africa. Clim. Dyn. 1–17. doi:10.1007/s00382-016-3296-z

Shukla, S., Sheffield, J., Wood, E.F., Lettenmaier, D.P., 2013. On the sources of global land surface hydrologic predictability. Hydrol. Earth Syst. Sci. 17, 2781.

Shukla, S., Steinemann, A.C., Lettenmaier, D.P., 2011. Drought Monitoring for Washington State: Indicators and Applications. J. Hydrometeorol. doi:10.1175/2010JHM1307.1

Shukla, S., Wood, A.W., 2008. Use of a standardized runoff index for characterizing hydrologic drought. Geophys. Res. Lett. 35.

Sima, S., Ahmadalipour, A., Tajrishy, M., 2013. Mapping surface temperature in a hyper-saline lake and investigating the effect of temperature distribution on the lake evaporation. Remote Sens. Environ. 136, 374–385.

Smith, A.B., Matthews, J.L., 2015. Quantifying uncertainty and variable sensitivity within the US billion-dollar weather and climate disaster cost estimates. Nat. Hazards 77, 1829–1851.

Svoboda, M., LeComte, D., Hayes, M., Heim, R., Gleason, K., Angel, J., Rippey, B., Tinker, R., Palecki, M., Stooksbury, D., Miskus, D., Stephens, S., 2002. The drought monitor. Bull. Am. Meteorol. Soc. doi:10.1175/1520-0477(2002)083<1181:TDM>2.3.CO;2

Trenberth, K.E., Dai, A., van der Schrier, G., Jones, P.D., Barichivich, J., Briffa, K.R., Sheffield, J., 2014. Global warming and changes in drought. Nat. Clim. Chang. 4, 17–22. doi:10.1038/NCLIMATE2067

Van Loon, A.F., 2015. Hydrological drought explained. Wiley Interdiscip. Rev. Water n/a-n/a. doi:10.1002/wat2.1085

Vicente-Serrano, S.M., García-Herrera, R., Barriopedro, D., Azorin-Molina, C., López-Moreno, J.I., Martín-Hernández, N., Tomás-Burguera, M., Gimeno, L., Nieto, R., 2015. The

Westerly Index as complementary indicator of the North Atlantic oscillation in explaining drought variability across Europe. Clim. Dyn. 1–19.

Wang, L., Yuan, X., Xie, Z., Wu, P., Li, Y., 2016. Increasing flash droughts over China during the recent global warming hiatus. Sci. Rep. 6.

Weibull, W., 1939. A statistical theory of the strength of materials. R. Swedish Inst. Eng. Res.

Whan, K., Zscheischler, J., Orth, R., Shongwe, M., Rahimi, M., Asare, E.O., Seneviratne, S.I., 2015. Impact of soil moisture on extreme maximum temperatures in Europe. Weather Clim. Extrem. 9, 57–67.

Xia, Y., Mitchell, K., Ek, M., Sheffield, J., Cosgrove, B., Wood, E., Luo, L., Alonge, C., Wei, H., Meng, J., 2012. Continental-scale water and energy flux analysis and validation for the North American Land Data Assimilation System project phase 2 (NLDAS-2): 1. Intercomparison and application of model products. J. Geophys. Res. Atmos. 117.

Xiao, M., Nijssen, B., Lettenmaier, D.P., 2016. Drought in the Pacific Northwest, 1920–2013. J. Hydrometeorol. 17, 2391–2404.

Yan, H., Moradkhani, H., Zarekarizi, M., 2017. A probabilistic drought forecasting framework: A combined dynamical and statistical approach. J. Hydrol. 548, 291–304.

Yan, H., Wang, S., Wang, J., Lu, H., Guo, A., Zhu, Z., Myneni, R.B., Shugart, H.H., 2016. Assessing spatiotemporal variation of drought in China and its impact on agriculture during 1982-2011 by using PDSI indices and agriculture drought survey data. J. Geophys. Res. Atmos.

Yuan, X., Roundy, J.K., Wood, E.F., Sheffield, J., 2015. Seasonal forecasting of global hydrologic extremes : System development and evaluation over GEWEX basins. Bull. Am. Meteorol. Soc. 96, 1895–1912. doi:10.1175/BAMS-D-14-00003.1

Zhai, J., Huang, J., Su, B., Cao, L., Wang, Y., Jiang, T., Fischer, T., 2017. Intensity–area–duration analysis of droughts in China 1960–2013. Clim. Dyn. 48, 151–168.

Zhao, T., Dai, A., 2015. The magnitude and causes of global drought changes in the twenty-first century under a low–moderate emissions scenario. J. Clim. 28, 4490–4512.

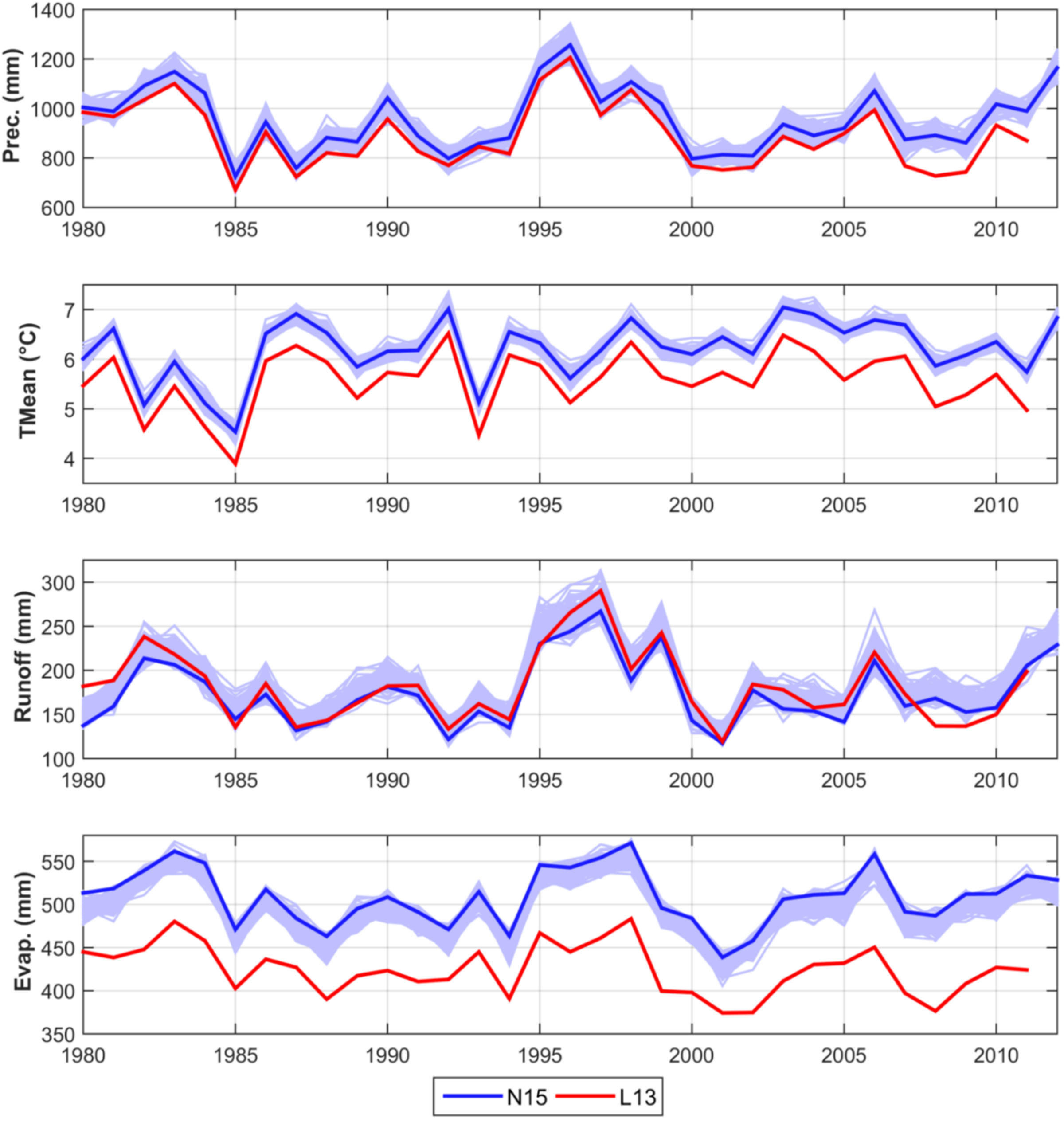
Prec. (mm)
TMean (°C)
Runoff (mm)
Evap. (mm)
1980
1985
1990
1995
2000
2005
2010
N15
L13

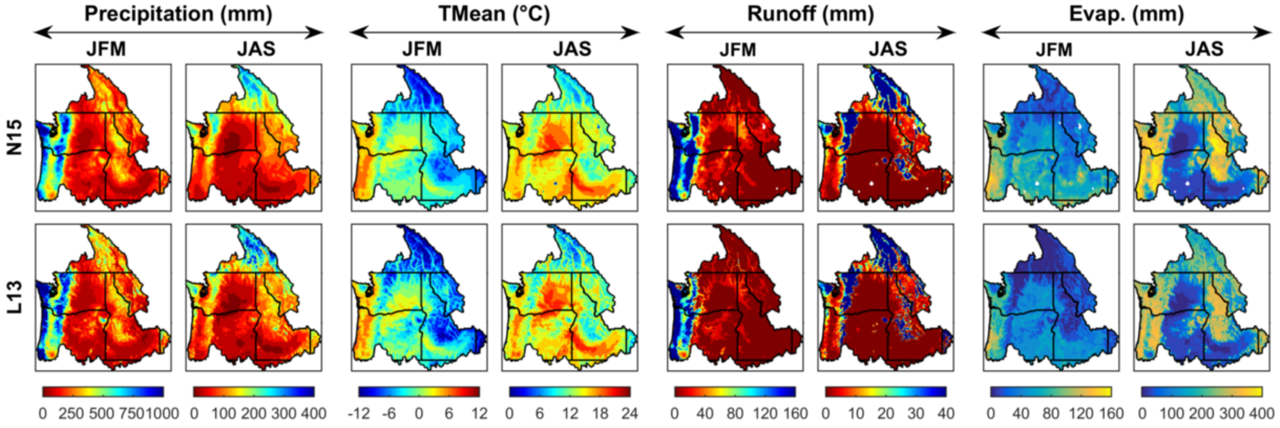

Precipitation (mm)
TMean (°C)
Runoff (mm)
Evap. (mm)
JFM
JAS
N15
L13
0 250 500 750 1000
0 100 200 300 400
-12 -6 0 6 12
0 6 12 18 24
0 40 80 120 160
0 10 20 30 40
0 40 80 120 160
0 100 200 300 400

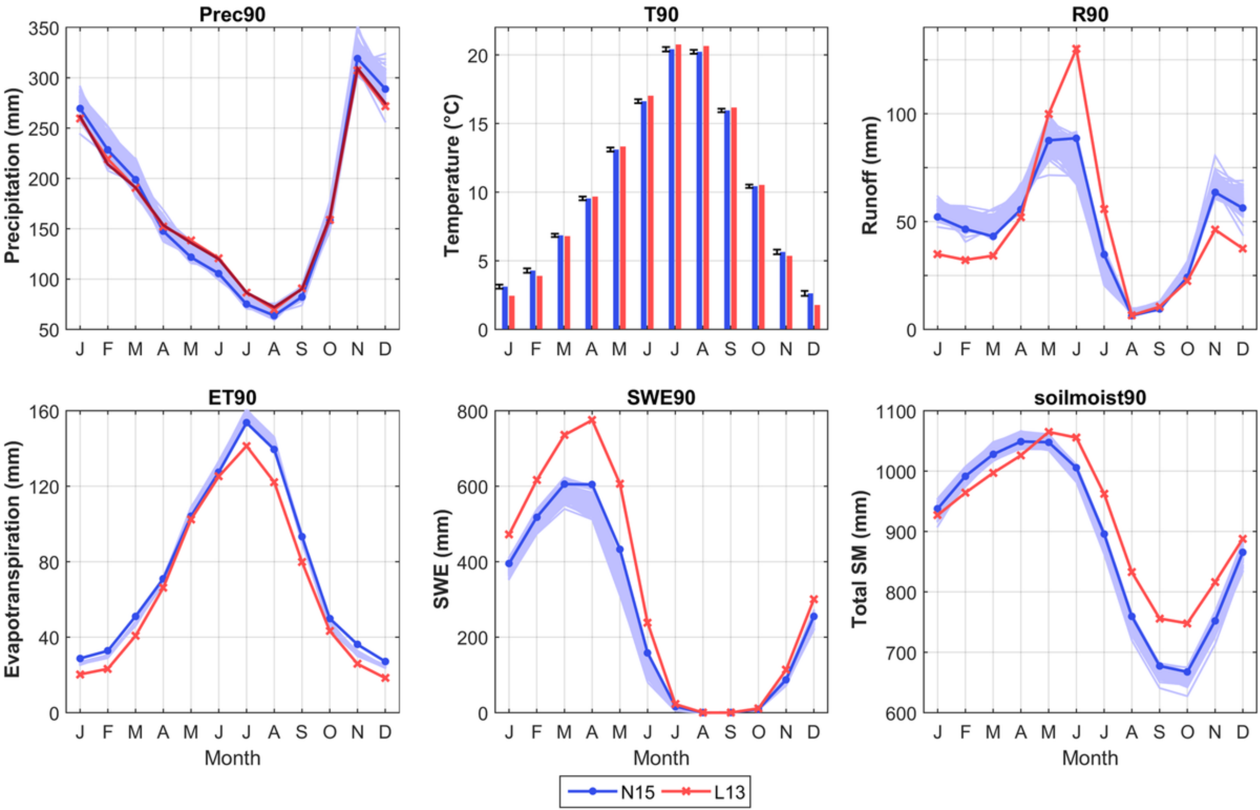

Prec90
Precipitation (mm)
350
300
250
200
150
100
50
J F M A M J J A S O N D
T90
Temperature (°C)
20
15
10
5
0
J F M A M J J A S O N D
R90
Runoff (mm)
100
50
0
J F M A M J J A S O N D
ET90
Evapotranspiration (mm)
160
120
80
40
0
J F M A M J J A S O N D
Month
SWE90
SWE (mm)
800
600
400
200
0
J F M A M J J A S O N D
Month
soilmoist90
Total SM (mm)
1100
1000
900
800
700
600
J F M A M J J A S O N D
Month
N15
L13

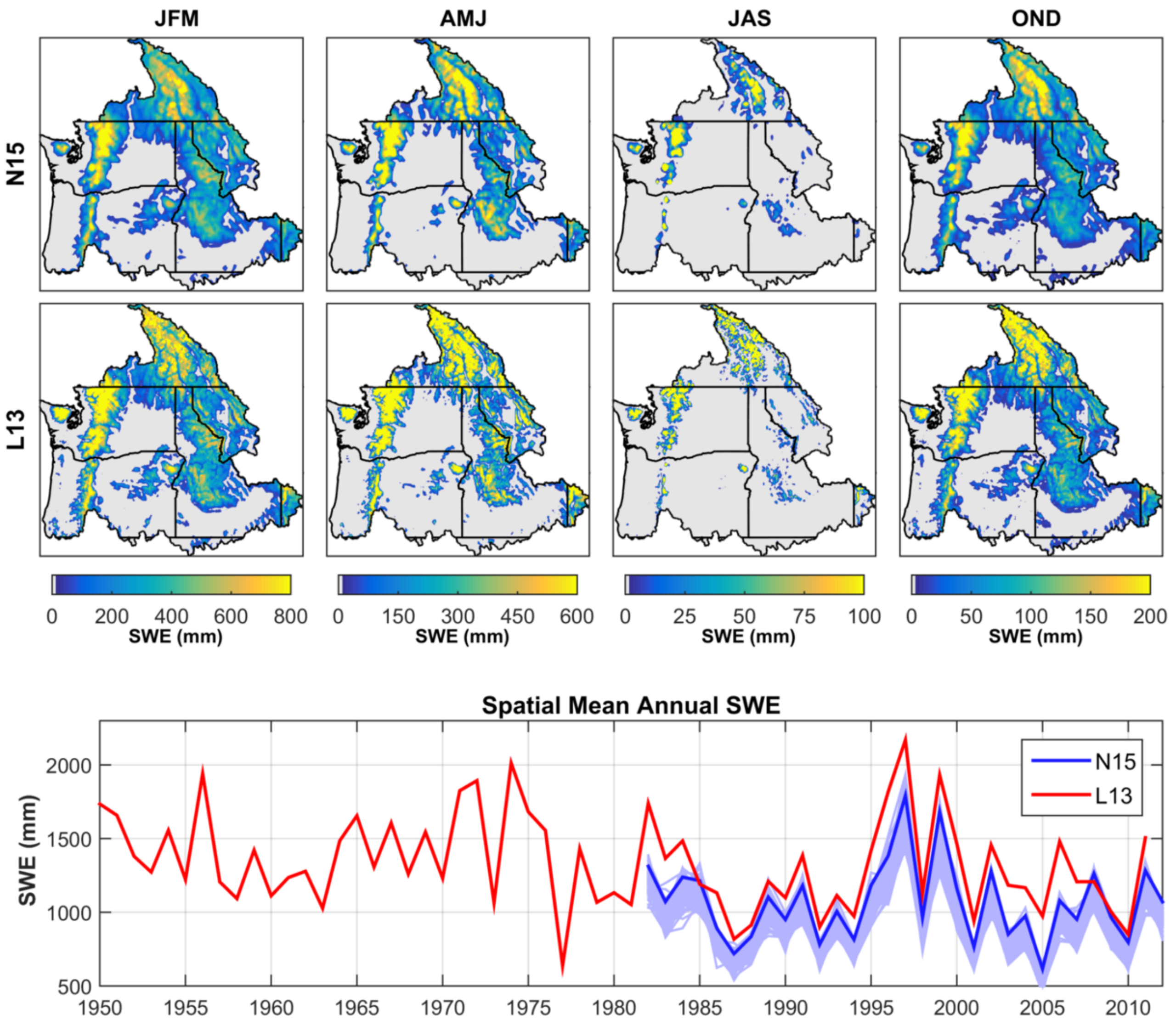

JFM
AMJ
JAS
OND
N15
L13
0 200 400 600 800
SWE (mm)
0 150 300 450 600
SWE (mm)
0 25 50 75 100
SWE (mm)
0 50 100 150 200
SWE (mm)
Spatial Mean Annual SWE
SWE (mm)
500
1000
1500
2000
1950 1955 1960 1965 1970 1975 1980 1985 1990 1995 2000 2005 2010
N15
L13

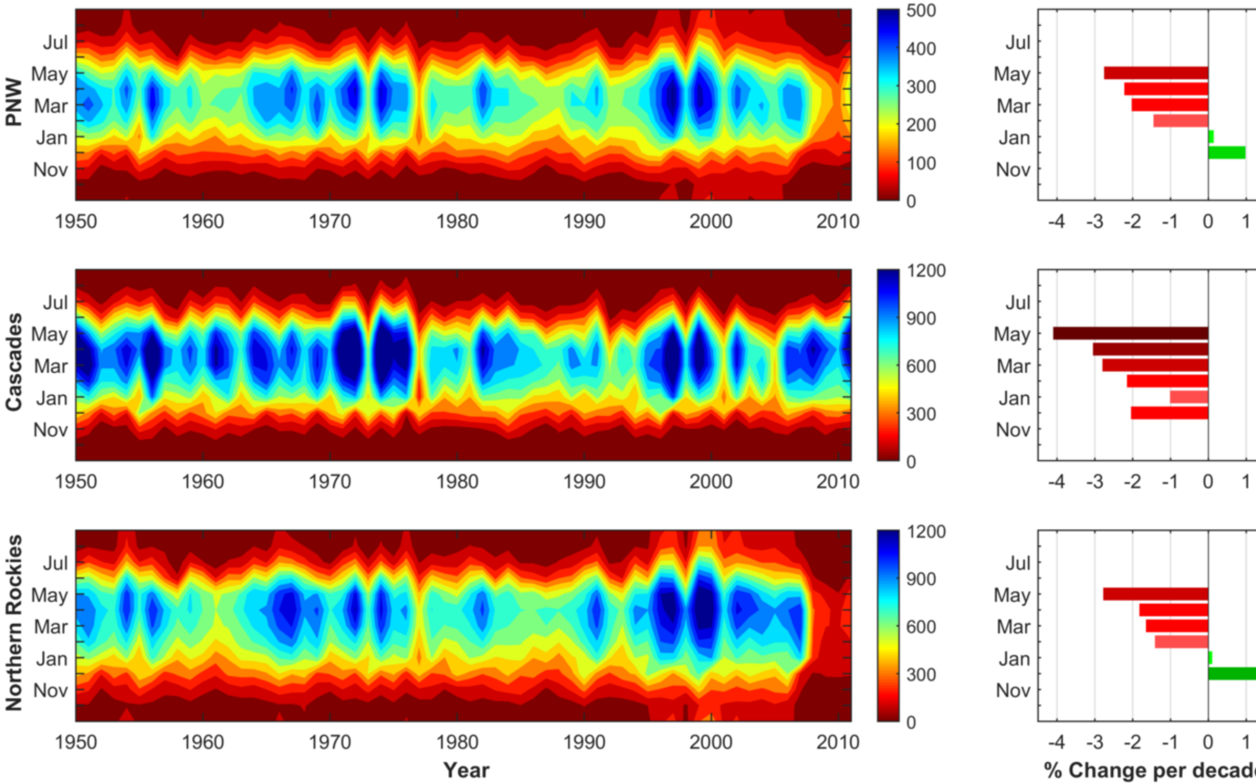
PNW
Cascades
Northern Rockies
Jul
May
Mar
Jan
Nov
1950
1960
1970
1980
1990
2000
2010
Year
500
400
300
200
100
0
1200
900
600
300
-4
-3
-2
-1
0
1
% Change per decade

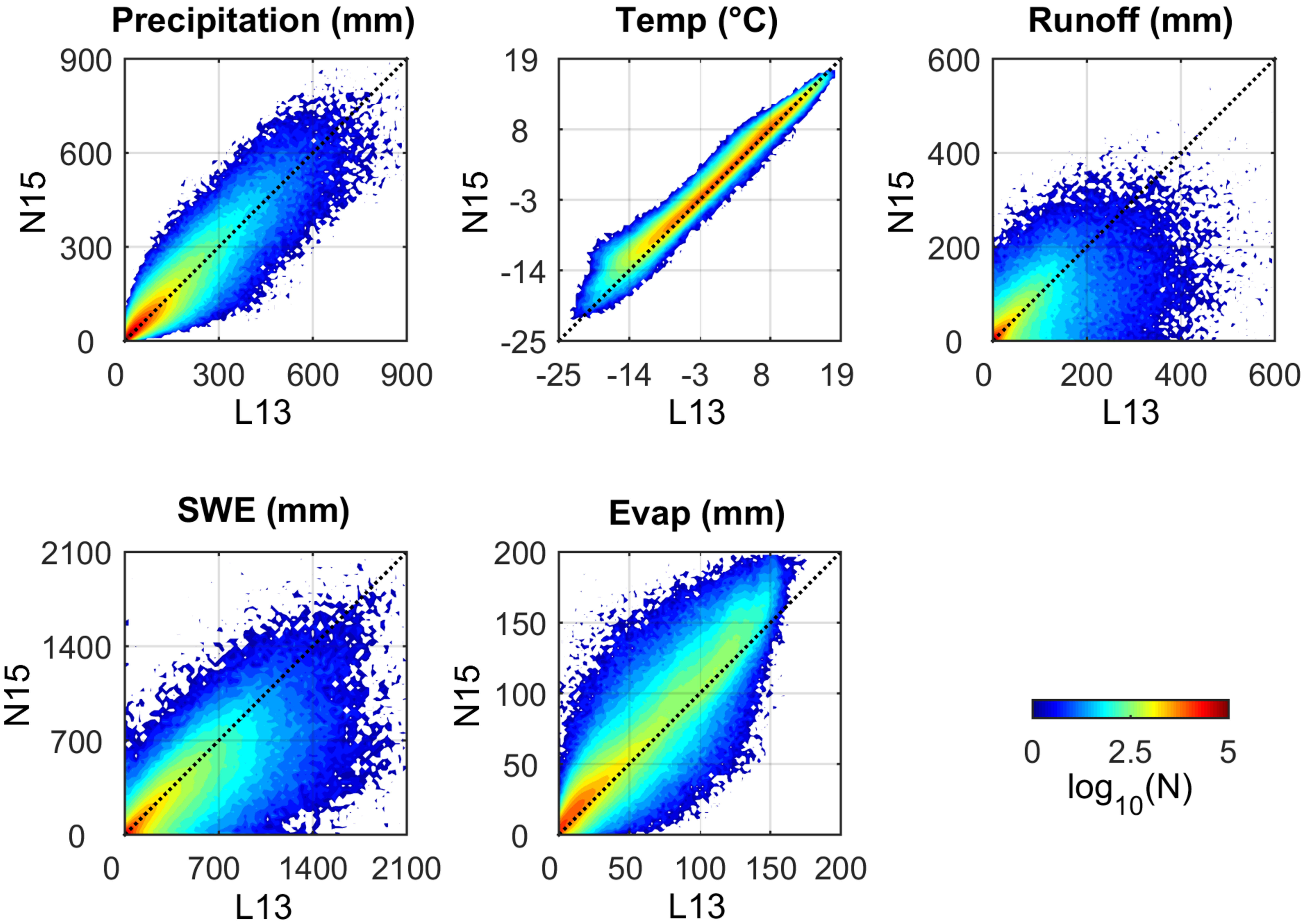

Precipitation (mm)
Temp (°C)
Runoff (mm)
SWE (mm)
Evap (mm)
N15
L13
0
300
600
900
-25
-14
-3
8
19
200
400
700
1400
2100
50
100
150
0
2.5
5
log10(N)

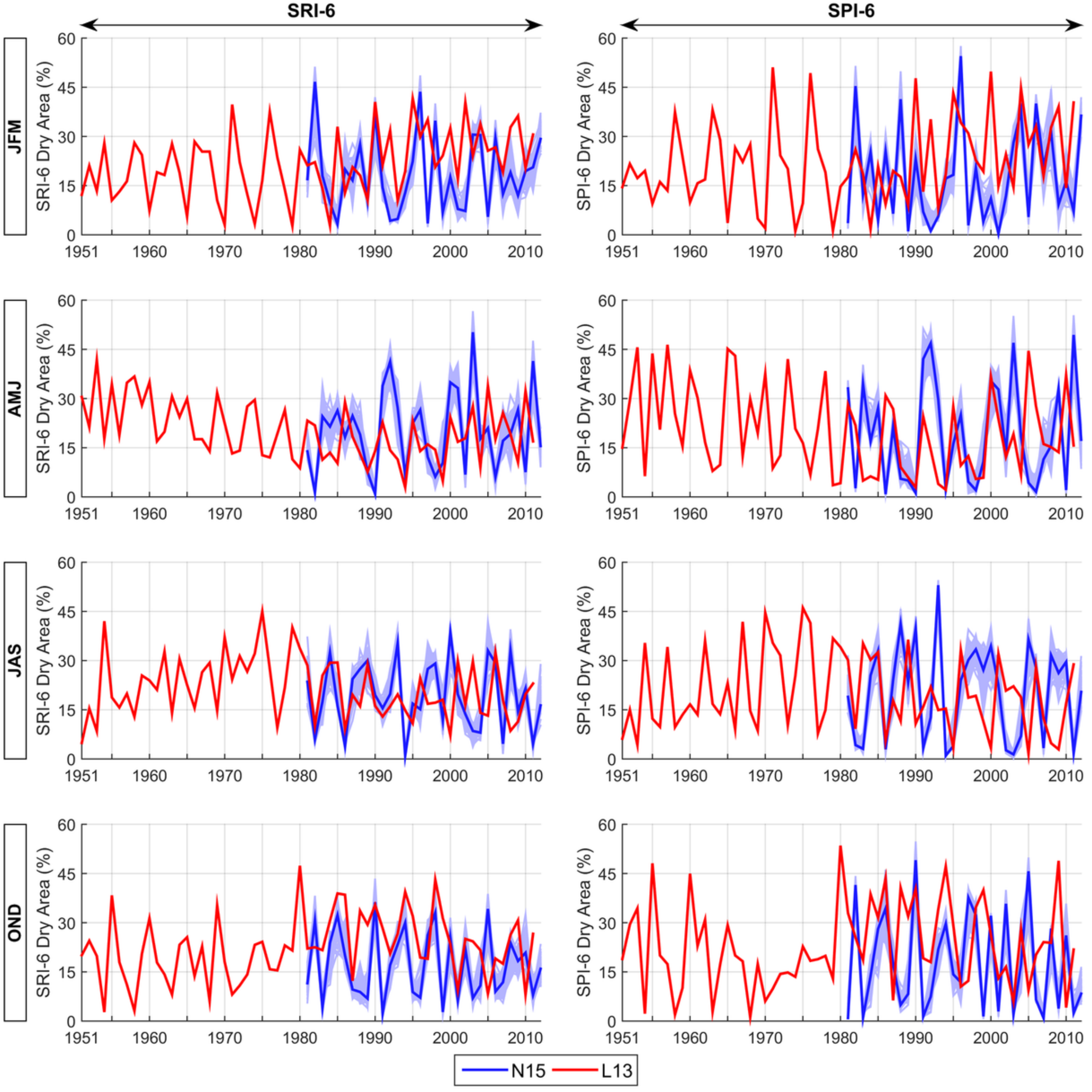
SRI-6
SPI-6
JFM
AMJ
JAS
OND
SRI-6 Dry Area (%)
SPI-6 Dry Area (%)
0
15
30
45
60
1951
1960
1970
1980
1990
2000
2010
N15
L13

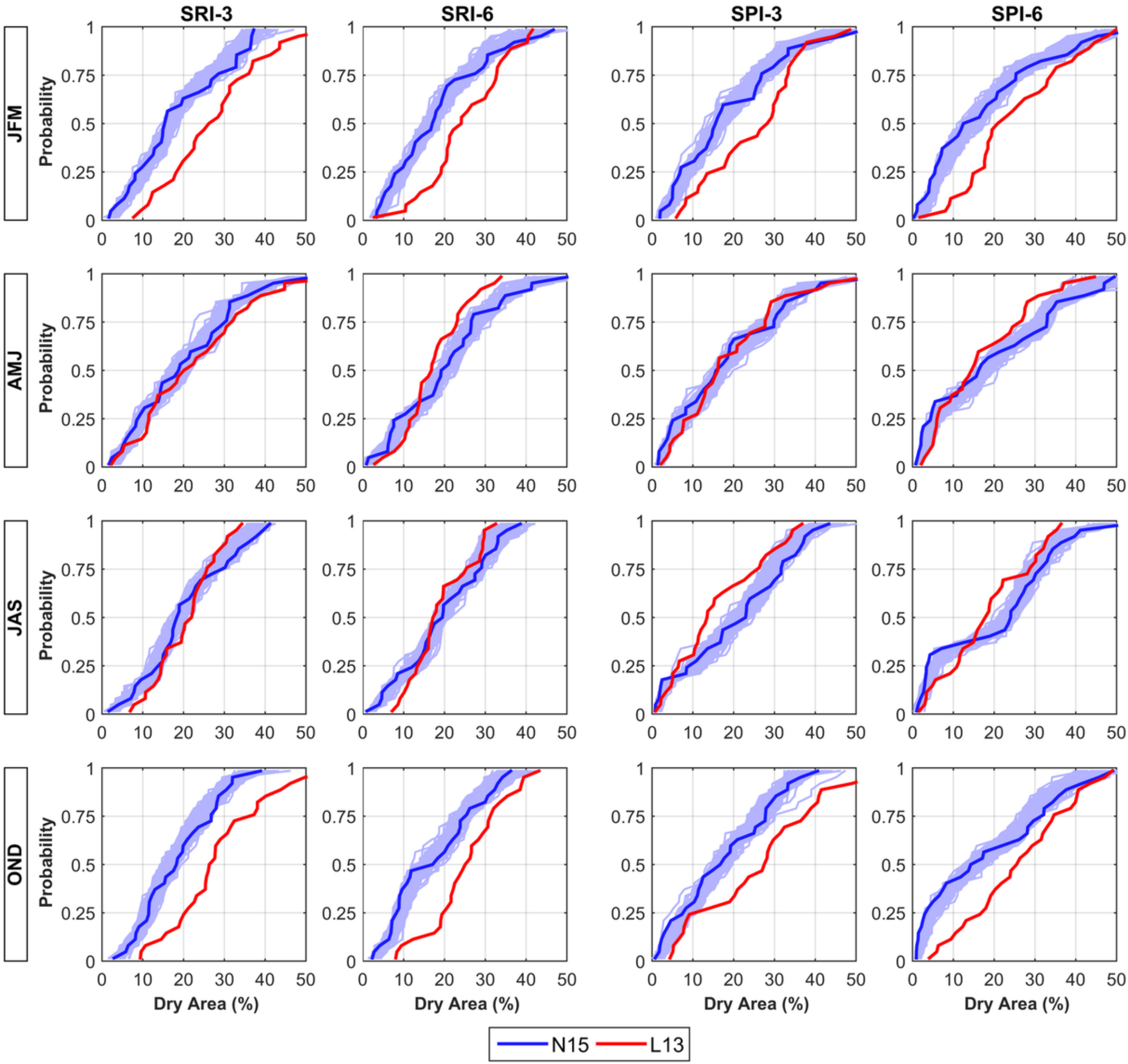

SRI-3
SRI-6
SPI-3
SPI-6
JFM
AMJ
JAS
OND
Probability
Dry Area (%)
N15
L13

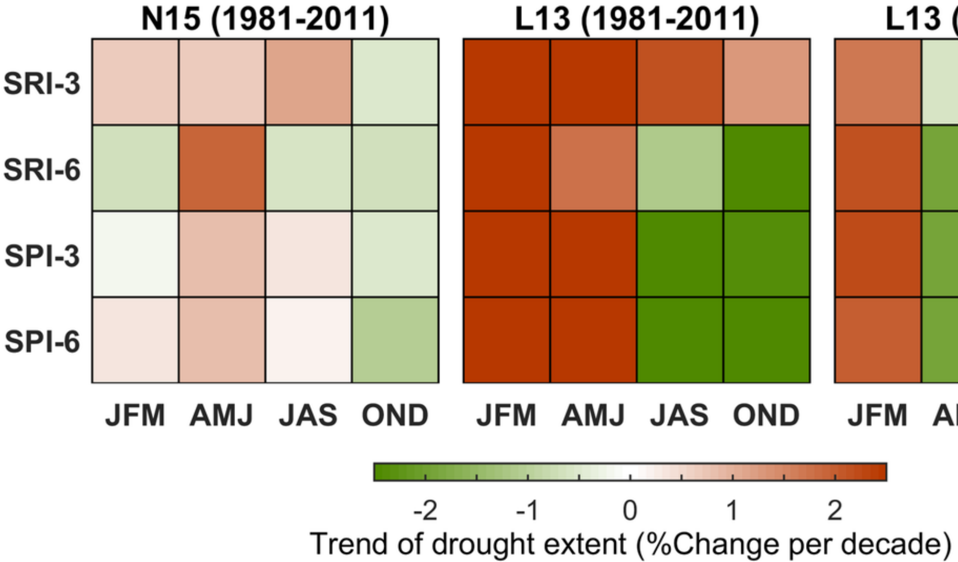
N15 (1981-2011)
L13 (1981-2011)
L13 (1951-2011)
SRI-3
SRI-6
SPI-3
SPI-6
JFM
AMJ
JAS
OND
-2
-1
0
1
2
Trend of drought extent (%Change per decade)

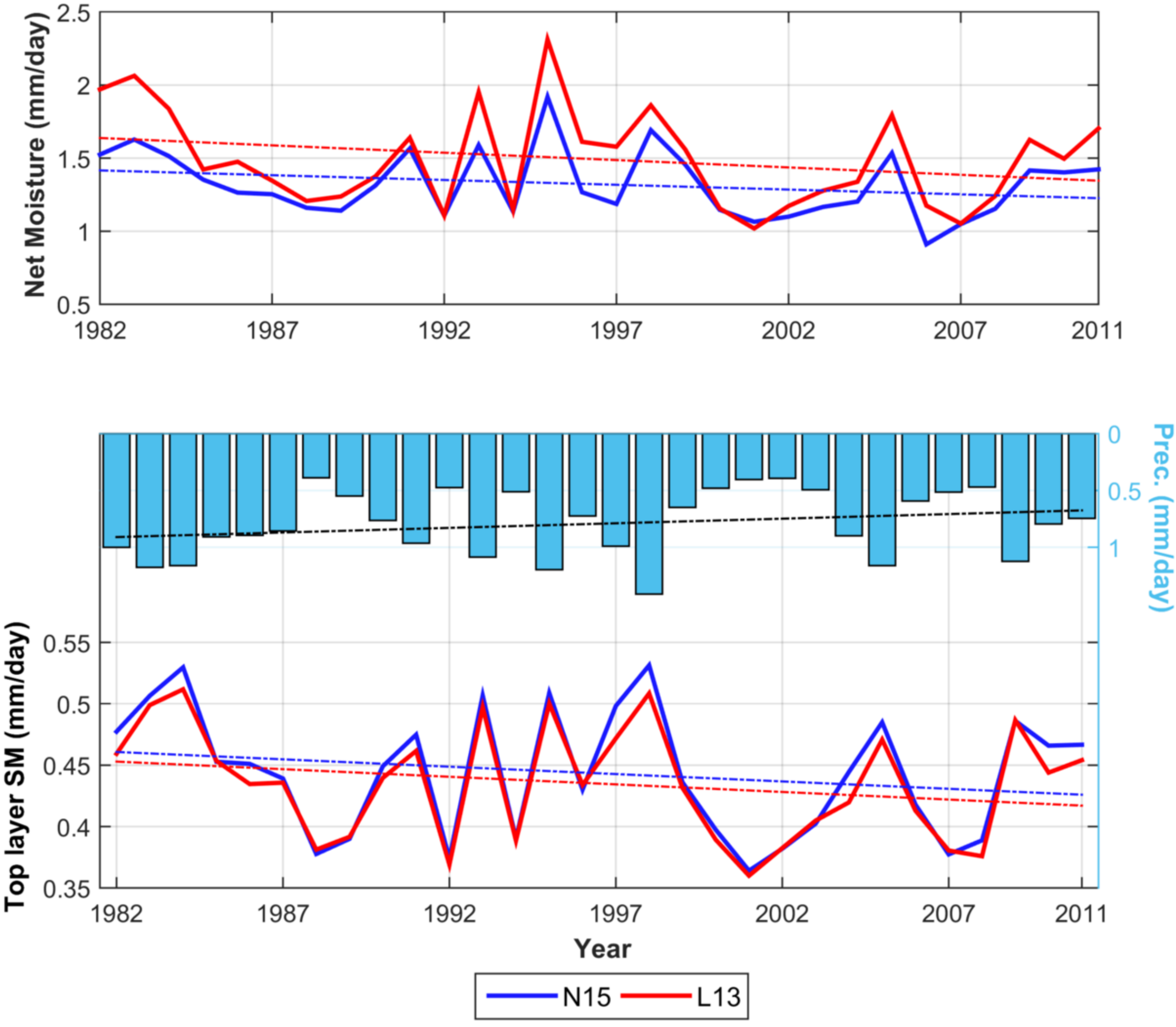

Net Moisture (mm/day)
2.5
2
1.5
1
0.5
1982
1987
1992
1997
2002
2007
2011
Prec. (mm/day)
0
0.5
1
Top layer SM (mm/day)
0.55
0.5
0.45
0.4
0.35
Year
N15
L13

Table 1. Summary of the characteristics of the gridded observation datasets utilized in this study; modified from Newman et al. (2015) and Henn et al. (2017).

Product	**Spatial resolution**	**Temporal resolution**	**Variables used**	**Ensemble members used**	**Precipitation data sources**	**Interpolation method**	**Reference**
L13	1/16° (~6 km)	Daily, 1950-2013	Prec. Tmax, Tmin, Wind	1	NWS COOP	Inverse distance	Livneh et al. (2013)
N15	1/8° (~12 km)	Daily, 1980-2012	Prec. Tmax, Tmin	100 + Ensemble mean	NWS COOP, NRCS SNOTEL, COCORAHS (GHCN-D)	Probabilistic	Newman et al. (2015)